BRAKING MOUNDS IN AVALANCHE SIMULATIONS - A SAMOSAT CASE STUDY

Andreas Kofler[1,*], Christian Tollinger[2], Annegret Jenner[2], Matthias Granig[2], Marc Adams[1]

[1] *Austrian Research Centre for Forests (BFW), Department of Natural Hazards, Innsbruck, Austria*
[2] *Austrian Service for Torrent and Avalanche Control (WLV), Innsbruck, Austria*

ABSTRACT: The town of Innsbruck is characterised by the mountain range ‘Nordkette’, which comprises some major avalanche tracks. The Arzler-Alm avalanche, reached the district of Mühlau in 1935. Since then, several generations of defence structures, such as braking mounds, as well as deflection and retention dams have been built. Several well-documented avalanche events allowed observing the effectiveness of the braking mounds in the Arzler-Alm run-out zone.

On the 21 January 2018 the Arzler-Alm avalanche released, nearly reaching the retention dam at the bottom of the run-out zone (1000 m a.s.l.). During the descent, the avalanche partly overflowed several braking mounds, located in the avalanche path and the run-out zone. These structures affected the avalanche flow. Aerial photographs were taken from manned and unmanned platforms over the release area and the deposition on 24 January 2018. They were used to map the affected area, thus providing a basis for the evaluation of the effectiveness of these defence structures and representing a well-documented case study for the simulation of dense snow avalanches and their interaction with defence structures.

Back calculations of the avalanche event were performed with SamosAT, considering the defence structures in different ways: a) braking mounds represented as part of the natural terrain by including a DTM with high spatial resolution (1 m ground sampling distance); b) areas with higher artificial resistance represent the braking mounds in the simulations. The simulations were compared to a reference simulation, where defence structures were omitted. Both investigated methods showed an influence on flow patterns and led to reduced avalanche velocities in the area next to the Arzler-Alm hut, compared to the reference simulation.

Keywords: avalanche simulation, defence structures, braking mounds

1. INTRODUCTION

The town of Innsbruck is characterised by the mountain range ‘Nordkette’. It rises from the outskirts of Innsbruck at 600 m to the ridge at about 2600 m a.s.l.. Several avalanches are known on this south-exposed mountain slope, some of them reaching the settlement area. One of the most threatening of these avalanches is the Arzler-Alm avalanche. Their release areas are located between the Hafelekarspitze (2,334 m) and the Gleirschspitze (2,317 m), leading to three individual flow paths, which unite in the Arzler-Alm area (1,067 m). The mean slope angle of the release area is about 40° (see figure 1).

Smaller avalanches reached the Hungerburgterrasse at about 950 m, the largest documented avalanche event hit the district of Mühlau in 1935. Since then, several generations of defence structures have been built. In the upper run-out zone energy dissipating structures were established in 1935 in terms of braking earth mounds, which later were reconstructed to concrete-stabilised wedges. In the fifties and sixties deflection measures were situated directly underneath and in the early seventies a huge catching dam was subsequently built, which defines the lower border of the today existing mitigation measures. Continuing avalanche activity allowed to reassess the effectiveness of the defence structures (WLV, 2017b,a).

The aim of this work is to assess the effectiveness of the braking mounds, both in theory and practice. Based on the documentation of the most recent avalanche event, which occured in January of 2018, the effectiveness of the braking mounds in the Arzler-Alm run-out zone is discussed. Furthermore the possibilities to include braking mounds in avalanche simulations with the software tool SamosAT is investigated.

2. THE AVALANCHE EVENT IN JANUARY 2018

On the 21[st] of January 2018, after a large snowfall event an avalanche released in the starting zone of the Almtal. During the descent, the avalanche partly overflew several braking mounds and deposited in

* Corresponding author address:
Andreas Kofler
Austrian Research Centre for Forests (BFW), Department of Natural Hazards, Rennweg 1, 6020 Innsbruck, Austria
Tel.: +43-512 573933 5175
Email: andreas.kofler@bfw.gv.at

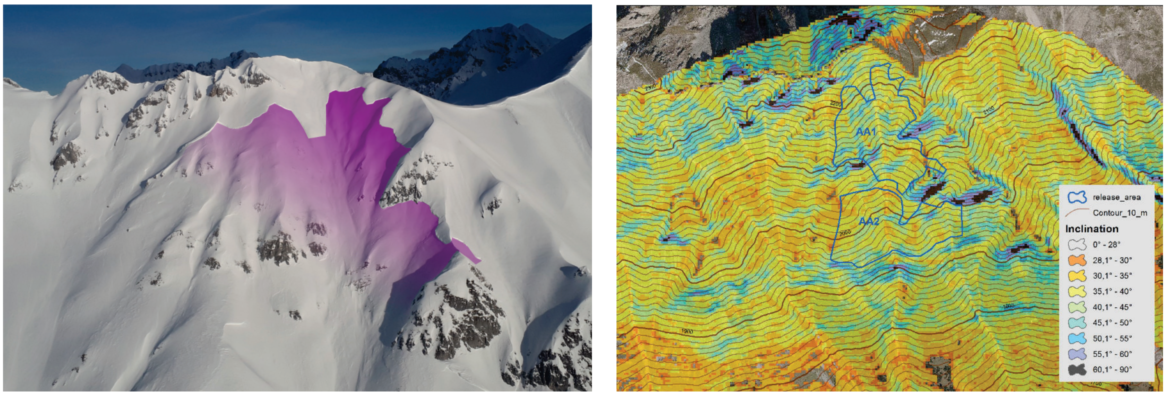

Figure 1: Photo (WLV, 2018) of the release (left) and inclination map (right).

the intermediate hutches. These structures affected the avalanche flow. As a consequence of the additional resistance in the path by horizontal and vertical obstacles, the snow mass decelerated and finally deposited, thus not reaching the retention dam at the bottom of the run-out zone (1000 m a.s.l.). A smaller avalanche, triggered in the Bruntal, reached the first braking mound. Compared to the extreme value analysis of Fischer et al. (2013) the avalanche has a return period below five years (projected run out distance $\approx$ 2300 m, fall height $\approx$ 1250 m).

Aerial photographs were taken from manned and unmanned platforms over the release area and the deposition on 24 January 2018. They were used to map the release areas (see figure 1) and affected area, thus providing a basis for the evaluation of the effectiveness of these defence structures. A detailed description about the documentation of the event can be found in Adams et al. (2018).

3. SIMULATION

Back calculations of the avalanche event were performed with SamosAT (Sampl, 2007; Oberndorfer and Granig, 2007), considering the defence structures in different ways: a) braking mounds represented as part of the natural terrain by including a DTM with high spatial resolution (1 m ground sampling distance); b) areas with higher artificial resistance represent the braking mounds in the simulations. The used flow model in SamosAT consists basically of (i) the mechanical description of the motion of the granular mass flow (mechanical model), which covers the basic conservation equations and (ii) additional closures (process models, e.g. frictional relation, entrainment). These are necessary to solve the main equations and calculate the temporal evolution of flow depth $\bar{h}$ and velocity $\bar{\mathbf{u}}$.

The governing equations are the conservation equations, namely the mass balance (1) and the momentum balance (2), which are formulated for an incompressible, isotropic material (ρ = const.), integrated over an infinitesimal control volume $V = A\,\bar{h}$.

$$\frac{\mathrm{d}V}{\mathrm{d}t} = \frac{\mathrm{d}(A\,\bar{h})}{\mathrm{d}t} = \dot{q}\,A. \tag{1}$$

$$\frac{\mathrm{d}\bar{u}_i}{\mathrm{d}t} = g_i + \frac{1}{A\,\bar{h}}\oint\limits_{\partial A}\left(\frac{\bar{h}\,\sigma^{(b)}}{2}\right)n_i\,\mathrm{d}l - \delta_{i1}\frac{\tau^{(b)}}{\bar{h}} - \frac{\bar{u}_i}{\bar{h}}\,\dot{q}\,. \tag{2}$$

For a detailed description of the respective terms we refer to Sampl (2007) and Fischer et al. (2015). It is noteworthy that entrainment has not been considered in any of the simulations, thus leading to an entrainment rate of $\dot{q} = 0$.

The simulations were compared to a reference simulation, where defence structures were omitted. The results of the simulations were compared to the mapped extent and depth of deposition, to qualitatively assess the different approaches of representing the defence structures in the simulation. Especially the flow behaviour over and around the man-made obstacles were of major interest.

3.1. Reference simulation

To perform a simulation run with the implemented flow model, we have to define the simulation input, such as release area and release height. For this investigation, only release areas for the relevant path have been assessed by expertise. A main release area with $A_{\mathrm{rel},1}$ = 4.5 ha and a secondary release area with $A_{\mathrm{rel},2}$ = 4.1 ha have been mapped using aerial photographs (see figure 1). Release heights of $d_{\mathrm{rel},1}$ = 1.0 m and $d_{\mathrm{rel},2}$ = 0.8 m were determined under the assumption, that the released volume $V_{\mathrm{rel}} = 77{,}000\ \mathrm{m}^3$ roughly reproduces the documented deposit volume ($V_{\mathrm{dep}} \approx 70{,}000\ \mathrm{m}^3$, see Adams et al., 2018). Thus, we assume a constant density and neglect the influence of densification, which would lead to a volume reduction up to a factor of two (Bartelt et al., 2012). Since no entrainment was considered, this presumption is acceptable.

Boundary conditions are normally provided through the DTM. The reference simulation was

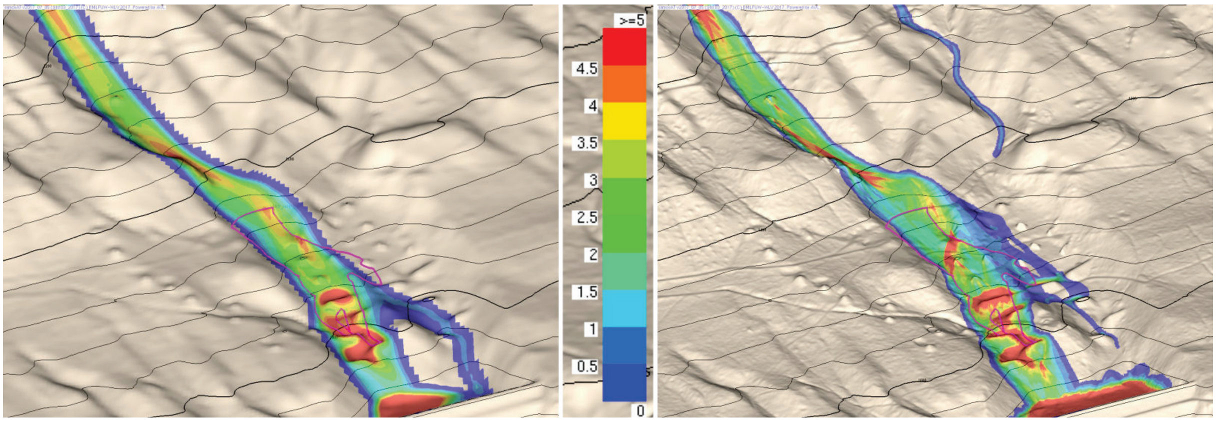

Figure 2: Reference simulation on DTM with a spatial resolution of $5\ \mathrm{m} \times 5\ \mathrm{m}$ (left) and simulation on a DTM with a higher spatial resolution of $1\ \mathrm{m} \times 1\ \mathrm{m}$. The colour indicates the peak flow depth result, ranging from 0 m (blue) to ≥ 5 m (red). Both simulation stop in the catching dam.

performed on a DTM with a spatial resolution of $5\ \mathrm{m} \times 5\ \mathrm{m}$, which should represent the winterly, snow covered terrain. Also the used process model parameters of SamosAT (v2017_07_05, Parameter Standard Std:03_2017) were optimized using this spatial resolution (Jörg and Granig, 2009; Sampl, 2015) and represent the standard settings for hazard zoning applications with SamosAT. The braking mounds are present in this digital representation of the terrain, but smoothed.

The result of the reference simulation can be seen in figure 2 (left). During its descent, the moving snow reaches a maximum velocity of ≈ 50 m/s, until the catching dam stops the avalanche. Thus the simulation does not reproduce the runout behaviour of the documented event, where most of the avalanche mass came to rest next to the Arzler-Alm hut (see Adams et al., 2018), although the mean flow depth $\bar{d}_{\text{flow}} = 2.8$ m ($d_{\text{flow,max}} = 10.3\ m$) over the documented deposition area is comparable to the documented deposition depths ($\bar{d}_{\text{dep,mean}} = 2.4$ m).

3.2. Simulation on DTM with higher spatial resolution

To better account for braking mounds in the simulations, we tried tu use a calculation raster with a higher spatial resolution of $1\ \mathrm{m} \times 1\ \mathrm{m}$ DTM. No additional resistance areas were considered.

The spatial resolution has a direct influence on the surface curvature. For this investigation, the profile curvature, which is the curvature in the direction of steepest slope has been analysed using QGIS. The curvature is expressed as $\frac{1}{m}$, positive values indicating convex and negative indicating concave landforms. The investigated area of interest lies next to the Arzler-Alm hut, where most of the braking mounds are located. The analysis shows that a smaller resolution leads to larger maximal (absolute values) curvatures up to a factor of five. This in turn means five times smaller curvature radii $\kappa = \frac{1}{R}$ for smaller resolution.

To better understand the consequences of a higher spatial resolution we take a look at the single components of the momentum conservation, i.e. equation (2). The first and the fourth term on the right hand side of equation (2), which describe the accelerations due to gravity with its components g_i and decelerations due to momentum loss of entrained mass ($\dot{q} > 0$) are not influenced by a change in curvature, but the second term and third term are affected by a change in curvature. Arising pressure gradients on the control volume V, with boundary line ∂A with elements $\mathrm{d}l$ and the normal vector n_i may change due to the change in the bottom stress. The frictional decelerations are directly linked to the bottom friction, as can be seen in the modified frictional relation of SamosAT in equation (3). Therein the basal shear stress τ_b is expressed by

$$\tau^{(b)} = \tau_0 + \mu \left(1 + \frac{R_s^0}{R_s^0 + R_s}\right) \sigma^{(b)} + \frac{\bar{\rho}\, \bar{\mathbf{u}}^2}{\left(\frac{1}{\kappa}\ \ln \frac{\bar{h}}{R} + B\right)^2}\,. \quad (3)$$

τ_0 represents a minimum shear stress, which has to be overcome for flowing ($\bar{\rho}\, \bar{h}\, g\, \sin\alpha > \tau_0$, with the inclination α), which by standard is deactivated ($\tau_0 = 0$). The fludization factor R_s is calculated with $R_s = \frac{\bar{\rho}\,\bar{\mathbf{u}}^2}{\sigma^{(b)}}$ and together with the empirical constant R_s^0, R_s affects the Coloumb friction force depending on velocity. Smaller velocities result in higher friction, especially in the runout zone. The last term describes the influence of the turbulent velocity profile and the resulting roughness on the bottom friction. Therein κ stands not for curvature, but represents the Karman constant.

A higher curvature, i.e. $\frac{\partial^2 \bar{z}}{\partial x_1^2} = \kappa = \frac{1}{R}$, generally leads to a higher normal stress at the bottom

$$\sigma^{(b)} = h\,(g_3 - \frac{\partial^2 \bar{z}}{\partial x_1^2}\, \bar{\mathbf{u}}^2)\,, \quad (4)$$

with the surface parallel velocity components $\bar{u}_1, \bar{u}_2$, the surface normal flow depth $\bar{h}$. g_3 describes the surface normal acceleration due to gravity and the curvature accounts for the change in the normal acceleration due to surface curvature in flow direction. Thus resolution has a direct impact on pressure gradients and the bottom shear stress $\tau^{(b)}$.

The simulation result of the simulation with a higher spatial resolution can be seen next to the reference simulation in figure 2 (right). From a qualitative viewpoint, the shown peak flow depths look very similar. Both simulations reach the catching dam at $\approx 80-85$ s and are stopped. Also the flow patterns look rather similar, with highest peak flow depths in the center of the flow path and right after the braking mounds and at the bottom of the catching dam.

When focusing at the documented deposition area in table 1, we note that both the the maximal velocities and also the mean velocities of the simulation with the higher resolution are lower than those of the reference simulation. On the contrary, a almost double as higher maximal peak flow depth of $19.5\ m$ was evaluated for the simulation with a higher spatial resolution, whereas the mean peak flow depths (2.8 m and 3.1 m) were of comparable size.

3.3. Simulation using resistance areas

A possibility to include braking mounds in avalanche simulations with SamosAT is to incorporate artificial resistance areas. For each of these classified resistance areas, a resistance force F_i^{res} is considered in the momentum balance. The respective term, which is added to the momentum conservation (2) is

$$\frac{F_i^{\text{res}}}{\bar{\rho}\, A\, \bar{h}} = C_{\text{res}}\, \bar{\mathbf{u}}^2\, \frac{\bar{u}_i}{||\bar{\mathbf{u}}||}\,, \tag{5}$$

with the effective resistance coefficient

$$C_{\text{res}} = \frac{1}{2}\,\bar{d}\,\frac{c_w}{s_{\text{res}}^2}\,.$$

This leads to a deceleration of avalanche mass in resistance areas, dependent on the respective flow velocity ($\bar{\mathbf{u}}^2$), obstacle geometry (mean diameter $\bar{d}$) and spatial distribution (s_{res}^2) of obstacles. Thus flow through resistance areas is not prevented (see figure 3 (left)), as the relation has primarily been developed for forested areas.

The location of the braking mounds in the simulations is based on the construction register of the Austrian Service for Torrent and Avalanche Control. The respective lateral lengths are about 10 m, their heights are approximately 5 m. Simulations with varying geometric aspects showed that the height (5 m, 10 m or more) has no major influence on the simulation result as long it is not easily overflown, but the lateral length is important as more or less

		max	mean	std
reference	pfd [m]	10.3	2.8	2.0
	pv [m/s]	31	20	7.7
resolution	pfd [m]	19.5	3.1	2.7
	pv [m/s]	29	17	5.7
resistance	pfd [m]	9.5	3.2	2.2
	pv [m/s]	25	16	6.4

Table 1: Evaluation of simulation results (**p**eak **v**elocities and **p**eak **f**low **d**epths) over the documented deposition area. The deposition area covers 609 cells for the 5 m grid and 15228 cells for the 1 m resolution.

cells of the calculation grid (cell size = 5 m) are overlapped. The resistance coefficient has been chosen to $c_w = 10$, leading to an effective resistance coefficient $C_{\text{res}} = 100$.

The results indicate that considering braking mounds in terms of resistance areas in SamosAT leads to realistic avalanche flow behaviour around the obstacles (see figure 3 (right)). The runout distance is not affected for this case study, since both simulations, with and without resistance areas stop in the catching dam and also the travel time to the catching dam is ≈ 80 s.

The maximal velocity over the whole simulation grid equals the maximal velocity of the reference simulation (≈ 50 m/s) and hence is not influenced by the resistance areas. This also means that the maximal velocity is reached at a certain point in the avalanche track above the first braking mound. The evaluation of the simulation results in the area of the documented deposit indicates that resistance areas do affect the respective velocities. Both, maximal and mean velocity are lower by ≈ 5 m/s than the respective velocities of the reference simulation. The peak flow depths are only slightly influenced.

4. CONCLUSIONS

Braking mounds have an influence on the dynamic behaviour of avalanches. In this work, different approaches to include such defence structures in avalanche simulations with SamosAT were investigated. The simulation input was derived from the documentation of the Arzler-Alm avalanche event from January 2018. Release areas were determined from aerial photographs and a photogrammetric evaluation of the avalanche track and run out area delivered an estimate of the deposit volume. From these two values, the release heights were derived, assuming that the release should approximately match the documented deposit volume. Thus we neglect densification, which would lead to a smaller deposit volume, but we also do not consider entrainment as a source of volume or mass growth.

Using the standard set up of SamosAT by the

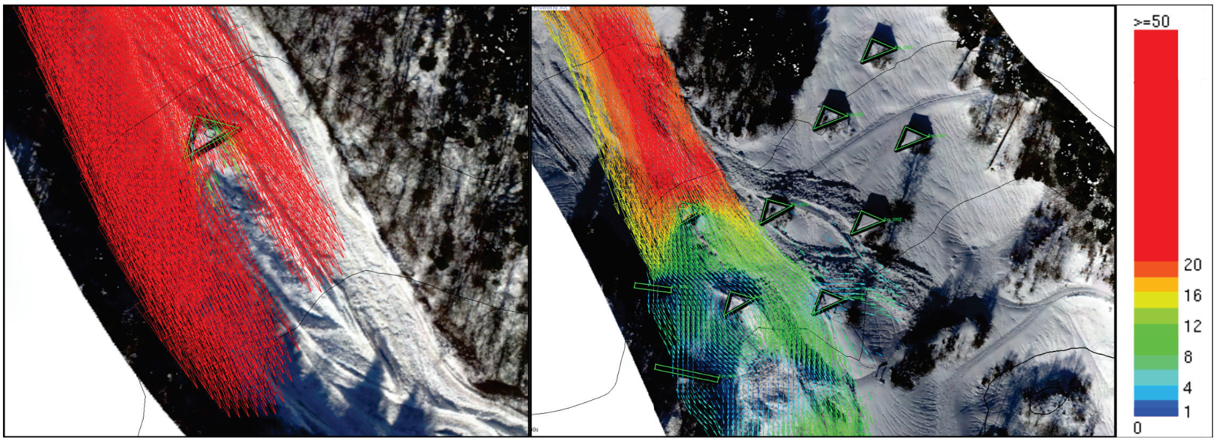

Figure 3: Velocity vectors of (left) SamosAT simulation with single braking mound in the avalanche path, timestep 48 s and (right) SamosAT Simulation with braking mounds in deposition zone, time step 80 s (right).

Austrian Service for Torrent and Avalanche Control (WLV) (Jörg and Granig, 2009; Sampl, 2015), a reference simulation to recalculate the documented avalanche event was set up. The simulation result overflow the documented deposit area and stopped in the catching dam. This can be connected to the fact, that the used process model parameter combination of SamosAT (v2017_07_05, Parameter Standard Std:03_2017) is used for hazard zoning, which is calibrated for avalanches with high return periods and different snow characteristics.

In order to better account for the braking mounds as a part of the natural terrain, we used a DTM with a higher spatial resolution. We supposed lower avalanche velocities due to terrain curvature and therefore a shorter run out length, but we observed higher maximal velocities in the avalanche track and also higher maximal flow heights. For the run out distance no change could be found, since the simulation terminated in the catching dam. But the resolution led to velocity vectors, which reproduced the observed flow patterns around the braking mounds and also the mean velocity in the deposit area was lower for the simulation with the high spatial resolution than with for the reference simulation. In order to compare the simulations with different DTM and different spatial resolutions objectively, also the process model parameters should be optimized for both cases.

Finally a simulation with artificial resistance areas was set up. Again, the run out distance could not be affected sufficiently in order to reproduce the documented event. But the simulation result showed promising trends regarding flow patterns and braking effects (lower velocities), if enough DFA-cells were considered. The Arzler-Alm avalanche proved to be a good example for the verify avalanche dynamics models, especially when considering interaction with defence structures.

ACKNOWLEDGEMENT

We thank Peter Sampl (AVL LIST GmbH) for his support regarding SamosAT and valuable comments on the manuscript.

REFERENCES

Adams, M. S., Fischer, J.-T., Kofler, A., Tollinger, C., Graf, A., Hoffmann, J., and Fromm, R. (2018). Investigating avalanche interaction with defence structures using unmanned aerial system photogrammetry. In International Snow Science Workshop, Innsbruck, Austria - 2018.

Bartelt, P., Bühler, Y., Buser, O., Christen, M., and Meier, L. (2012). Modeling mass-dependent flow regime transitions to predict the stopping and depositional behavior of snow avalanches. Journal of Geophysical Research, 117(F1):F01015.

Fischer, J. T., Kofler, A., Fellin, W., Granig, M., and Kleemayr, K. (2015). Multivariate parameter optimization for computational snow avalanche simulation. Journal of Glaciology, 61(229):875–888.

Fischer, J.-T., Stepanek, L., Huber, A., Fromm, R., Zeidler, A., and Kleemayr, K. (2013). Extreme value analysis of design events. In International Snow Science Workshop, Grenoble Chamonix Mont-Blanc - 2013.

Jörg, P. and Granig, M. (2009). Kalibrierung der Widerstandsparameter in SamosAT. interner bericht, WLV-Stabstelle Schnee und Lawinen (SSL).

Oberndorfer, S. and Granig, M. (2007). Modellkalibrierung des Lawinensimulationsprogramms SamosAT. interner bericht, Forsttechnischer Dienst für Wildbach-und Lawinenverbauung, Stabstelle Schnee und Lawinen, Schwaz.

Sampl, P. (2007). SamosAT Modelltheorie und Numerik. Technical report, AVL List GMBH.

Sampl, P. (2015). Abschlussbericht: Erweiterung der Lawinensimulationssoftware SamosAT - Parallelisierung des Staublawinenteiles. Technical report, AVL List GMBH, Graz.

WLV (2017a). Arzler alm-lawine, gefahrenzonenplan innsbruck. Technical report, Forsttechnischer Dienst für Wildbach- und Lawinenverbauung, Innsbruck.

WLV (2017b). Arzler alm-lawine, vorprojekt 2017. Technical report, Forsttechnischer Dienst für Wildbach- und Lawinenverbauung, Innsbruck.